2021 43rd Annual International Conference of the
IEEE Engineering in Medicine & Biology Society (EMBC)
Oct 31 - Nov 4, 2021. Virtual Conference

Compartmental models for diffusion weighted MRI reveal widespread brain changes in HIV-infected patients

Silvia Minosse[1], Eliseo Picchi[1,2], Francesca Di Giuliano[3], Francesco di Ciò[1], Chiara Adriana Pistolese[2], Loredana Sarmati[4], Elisabetta Teti[4], Massimo Andreoni[4], Roberto Floris[2], Maria Guerrisi[1], Francesco Garaci[3,5], Nicola Toschi[1,6], Senior *Member, IEEE*

Abstract— **Diffusion tensor imaging (DTI) has been used to explore changes in the brain of subjects with human immunodeficiency virus (HIV) infection. However, DTI notoriously suffers from low specificity. Neurite orientation dispersion and density imaging (NODDI) is a compartmental model able to provide specific microstructural information with additional sensitivity/specificity. In this study we use both the NODDI and the DTI models to evaluate microstructural differences between 35 HIV-positive patients and 20 healthy controls. Diffusion-weighted imaging was acquired using three b-values (0, 1000 and 2500 s/mm^2). Both DTI and NODDI models were fitted to the data, obtaining estimates for fractional anisotropy (FA), mean diffusivity (MD), radial diffusivity (RD), axial diffusivity (AD), neurite density index (NDI) and orientation dispersion index (ODI), after which we performed group comparisons using Tract-based spatial statistics (TBSS). While significant group effects were found in in FA, MD, RD, AD and NDI, NDI analysis uncovered a much wider involvement of brain tissue in HIV infection as compared to DTI. In region-of interest (ROI)-based analysis, NDI estimates from the right corticospinal tract produced excellent performance in discriminating the two groups (AUC = 0.974, sensitivity = 90%; specificity =97%).**

Clinical Relevance—**The NODDI model combines additional sensitivity with built-in specificity, and provide additional information about the microstructural changes in multimodal areas involved in attentive, emotional and memory networks which are impaired in HIV patients.**

I. Introduction

Diffusion Weighted Magnetic Resonance Imaging (MRI) techniques play a key role in e.g. characterizing neoplastic tissues, to assess abnormalities in neurodegenerative diseases, and to predict and monitor response to therapeutic treatment [1]–[5]. Diffusion Weighted Imaging (DWI) is sensitive to the random movement of water molecules within tissue and consequently to microstructural tissue features [6]. Diffusion tensor imaging (DTI) can detect degeneration of the central nervous system (CNS) based on the assumption that the movement of water molecules within tissues is described by a Gaussian distribution [7], [8]. However, in biological tissues, there are cellular and macromolecular structures that affect the free diffusion of water molecules [9]–[12]. An alternative approach is to use biophysical models of the MRI diffusion signal to obtain more specific biomarkers of tissue microstructure. The neurite orientation dispersion and density imaging (NODDI) [13] is a biophysical models that can be fitted using data compatible with clinically feasible scan times. It can provide estimates of fiber density, orientation dispersion and distribution of axonal diameters. NODDI is a three-compartment model [14]: (a) intra-neurite compartment, which is represented by axons and is modelled as a collection of infinitely thin sticks; (b) extra-neurite compartment, including microglia, astrocytes, oligodendrocytes, neuronal cell bodies, ependymal cells, extra-cellular matrices, and vascular structures; (c) a free-water compartment, modeled as isotropic diffusion. Two main tissue parameters can be obtained after model fitting: the orientation dispersion index (ODI) and the neurite density index (NDI). ODI is sensitive to neurite dispersion, from strictly parallel to completely dispersed (higher ODI relates to greater neurite dispersion). In contrast, NDI is related to the number of neurites in a voxel (higher NDI relates to a higher number of [15]). NODDI has been used to study various clinical conditions such as brain tumors, epilepsy, Alzheimer's disease, traumatic brain injury, multiple sclerosis and stroke [16]–[21]. In all these studies, NODDI provided additional information compared to the DTI model. In addition, the ability of NODDI to characterize tissue microstructure was demonstrated through histological findings [20].

Several diffusion techniques have been used to assess morphological and structural changes in the CNS of HIV-infected patients and to monitor the course of the disease [22]–[26]. The HIV infects the CNS and can affect the neuronal networks, damaging the white and grey matter [27]. In this context, it has been shown that HIV-positive patients develop cognitive impairment. These abnormalities are correlated with diffusion imaging metrics that are able to study alterations in brain microstructure [28], [29]. The aim of the study is to explore microstructural brain changes in HIV patients using to gain more insight about compartmental-specific changes in microstructure due to HIV infection. An overall workflow of the study is shown in Figure 1.

[1]Department of Biomedicine and Prevention, University of Rome "Tor Vergata", Rome, Italy.
[2]Diagnostic Imaging Unit, Department of Biomedicine and Prevention, University of Rome Tor Vergata, Rome, Italy.
[3]Neuroradiology Unit, Department of Biomedicine and Prevention, University of Rome "Tor Vergata", Rome, Italy.
[4]Clinical Infectious Diseases, Tor Vergata University, Rome, Italy.
[5]San Raffaele Cassino, Frosinone, Italy.
[6]Athinoula A. Martinos Center for Biomedical Imaging, Harvard Medical School, Boston, MA, United States.

978-1-7281-1178-0/21/$31.00 ©2021 IEEE

II. METHODS

A. Participants

The Department of Infectious Diseases of the University Hospital Rome 'Tor Vergata' enrolled a total of 55 subjects composed (35 HIV-positive patients and 20 healthy controls. The present study was authorized by the hospital ethics committee. Inclusion criteria: (a) a previous HIV infection and (b) no clinical evidence of neurological disorders. Exclusion criteria: (a) history of head trauma, (b) stroke, (c) epilepsy, (d) CNS infections, (e) demyelinating disease, (f) tumors, (g) coinfections, (h) or any kind of contraindication to MRI examinations. The HIV-positive patients were made up by 27 men and 8 women, with an average age of 41.3 years (range 24–65 years). Healthy controls were made up by 11 men and 9 women, with an average age of 44.1 years (range 27–64 years). There were no statistically significant differences between the groups regarding either in age ($p = 0.46$, Mann–Whitney-U-Test) or gender ($p = 0.08$, Chi-Square Test).

B. MR Imaging protocol

MR imaging was performed with a 3T system (Achieva 3T Intera, Philips Healthcare, Best, The Netherlands), using 8 channel phased array head coil. Gradients amplitude and rise time were 80 mT/m and 200 mT/m/ms, respectively. For all subjects, the MRI acquisition protocol included: axial T2-weighted TSE sequence, axial T2-fluid attenuated inversion recovery, sagittal T1-weighted turbo spin echo sequence, and a T1-3D fast field echo sequence, which were used by an expert neuroradiologists to exclude visible abnormalities. Diffusion-weighted imaging were acquired using a spin-echo (SE) echo-planar (EPI) single-shot sequence with the following parameters: acquisition matrix, 94 × 94; field of view, 24 x 24 cm^2; repetition time/echo time, 7774 ms/89 ms; slice thickness, 2.5 mm; slices, 60; no gap. Three different *b* values (0, 1000, 2500 s/mm^2) were used. Thirty-two noncoplanar and noncollinear directions were chosen for the diffusion-weighed imaging (b = 1000, 2500 s/mm^2) and eight non-diffusion-weighted reference images (b = 0 s/mm^2) were also collected. The SENSE (SENSitivity Encoding) imaging option with a scan time reduction factor of 2 was used.

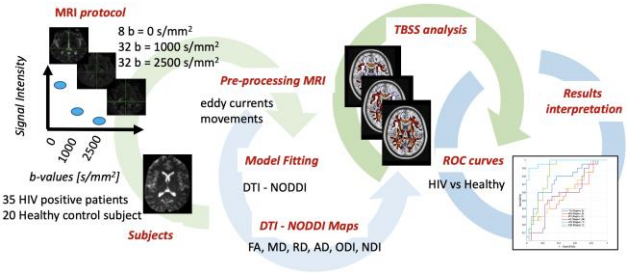

Figure 1. Overall workflow of the study

C. MR imaging data preprocessing and model fitting

Diffusion weighted images were preprocessed using the *eddy* tool, part of FSL (FMRIB Software Library v. 6.0.4, Oxford, UK) [30], to correct for subject motion and eddy currents. The Microstructure Diffusion Toolbox (MDT) using the Cascade Initialized optimization strategy [31], [32] was used to analyze DTI and NODDI models through a Powell optimization procedure. The diffusion-weighed imaging with b values = 0 and 1000 s/mm2 were used to fit the DTI model and obtain FA, MD, RD, and AD maps. All b values (0, 1000, 2500 s/mm2) were used to fit the NODDI model, hence obtaining the NDI and ODI maps. Successively, Regions of Interest (ROI) were defined using the ICBM-DTI-81 white-matter labels Atlas [33] (48 ROIs across the whole brain) and mean values for all indices were calculated within each ROI.

D. Statistical analysis

Tract Based Spatial Statistics (TBSS) [34] (part of FSL) was used for voxel-wise group comparison of all parameters. The TBSS analysis consists of the following steps: (a) nonlinear registration of all FA images with each other; (b) identification of the most representative FA image and use of this as the target image; (c) affine alignment of the target image in the Montreal Neurological Institute (MNI) 152 standard space; (d) transformation of each image into the MNI152 1x1x1mm3 space by combining the nonlinear transformation of the target FA image with the affine transformation from that target to the MNI152 space; (e) creation of mean of all FA images; (f) threshold at 0.2 and thinning to create an average FA skeleton, (g) projection of each subject's aligned FA data onto this skeleton. Successively, all previously computed warps are applied to all maps (MD, RD, AD, NDI and ODI), warping them into MNI space for subsequent skeletonization as above. The skeletonization step improves robustness against between-subject registration errors. Resulting data were then fed into voxel wise inter-subject, non-parametric statistics using randomize, also part of FSL. For all diffusion-derived metrics (DTI and NODDI), we tested the null hypothesis of no differences between HIV positive patients and healthy controls subjects using separate general linear models (GLMs), which included age and gender as nuisance covariates and correction for multiple comparisons over space using permutation-based nonparametric inference within the framework of the GLM (10,000 permutations) and using the Threshold-Free Cluster Enhancement (TFCE) [35], which eliminates the need for an arbitrary cluster threshold definition. A corrected p-value < 0.05 was assumed to be statistically significant. After TBSS, for each metric we also calculated the percentage of voxels (out of the whole skeleton) in which a significant effect was found. Finally, separate receiver operating characteristic (ROC) curves analysis was employed for each ROI and each metric to quantify the discrimination potential between HIV positive patients and healthy controls. For each ROC curve, the following parameters were evaluated: sensitivity, specificity, positive predicted value (PPV) and negative predicted value (NPV). The Kruskal-Wallis test and a post–hoc test with Bonferroni correction were used to determine if there were significant differences in ROC curve-related parameters across diffusion metrics.

III. RESULTS

TBSS results (Figure 2) showed lower FA and NDI values in HIV positive patients compared to controls. In particular, we observed lower FA values in HIV patients with moderate prevalence in the right brain hemisphere along the uncinate and superior longitudinal fasciculi, along the tight inferior frontal-occipital bundle, left forceps minor and in the cingulate gyrus. MD, RD and AD values were higher in HIV positive patients as compared to healthy subjects. In the same comparison, MD and RD metrics showed higher values along the cingulate gyrus, right superior longitudinal fasciculus and along the U-fibers with slight right brain hemisphere

prevalence; moreover, RD values were higher at the ganglionic level, and AD showed lower values in the right brain hemisphere along the inferior longitudinal fasciculus, the cortico-spinal tract, the temporal part of the superior longitudinal and uncinate fasciculi. NDI analysis disclosed a less focal and wider involvement of brain tissue as compared to DTI metrics. In particular, lower NDI values were found in HIV infected patients (as compared to controls) along the cortico-spinal tract, cerebellar hemispheres and vermis, in the occipital lobes, along the brainstem and along the white matter of the frontal lobes. No statistically significant differences in ODI were detected between the two groups. Also, the overall percentage of volume (across the TBSS skeleton) in which we found statistically significant differences between HIV patients and healthy controls was greatest in NDI (Table I.)

TABLE I. STATISTICALLY SIGNIFICANT DIFFERENCES BETWEEN HIV PATIENTS AND HEALTHY CONTROLS

Maps	%	Figure
FA	14.32	2 (a)
MD	24.97	2 (b)
RD	27.33	2 (c)
AD	11.00	2 (d)
NDI	59.16	2 (e)

% = % of voxels (out of whole skeleton) where we found significant group effects. Fractional anisotropy (FA), mean diffusivity (MD), radial diffusivity (RD), axial diffusivity (AD), neurite density index (NDI).

ROC analysis demonstrated the higher discrimination ability of NDI (Figure 3, Table II). The median AUC values across ROIs were noticeably higher in NDI as compared to all other indices. Also, Figure 4 sample ROC curves for the ROI which, in each index, produced the highest AUC value. As an example, NDI values in the right corticospinal tract (region 7) produced the best performance overall (AUC = 0.974, sensitivity = 90%; specificity =97%, PPV= 95%, NPV=94%).

TABLE II. MEAN AND STANDARD DEVIATION OF ROC CURVE PARAMETERS FOR DIFFUSION MAPS.

Maps	AUC	Sen	Spec	PPV	NPV
FA	0.62[0.54-0.68]	0.70 [0.60-0.75]	0.59[0.51-0.66]	0.48[0.43-0.54	0.76[0.72-0.80]
MD	0.34[0.29-0.38]	0.55[0.45-0.70]	0.37[0.26-0.49]	0.34[0.31-0.37]	0.60[0.56-0.65]
RD	0.33[0.29-0.38]	0.55[0.40-0.66]	0.37[0.26-0.51]	0.34[0.31-0.37]	0.60[0.55-0.64]
AD	0.39[0.33-0.42]	0.665[0.55-0.75]	0.39[0.31-0.46]	0.37[0.34-0.38]	0.64[0.59-0.68]
ODI	0.52[0.45-0.60]	0.63[0.55-0.70]	0.54[0.43-0.63]	0.42[0.39-0.48]	0.71[0.67-0.74]
NDI	0.82[0.72-0.88]	0.78[0.75-0.85]	0.77[0.66-0.86]	0.67[0.56-0.76]	0.86[0.82-0.91]

Sensitivity (Sen), specificity (Spec), positive predicted value (PPV) and negative predicted value (NPV), fractional anisotropy (FA), mean diffusivity (MD), radial diffusivity (RD), axial diffusivity (AD), neurite density index (NDI) and orientation dispersion index (ODI).

In addition, ROC curve parameters were significantly different (post-hoc comparisons) across metrics. (Table III)

TABLE III. SIGNIFICANT DIFFERENCES IN ROC CURVE PARAMETERS BETWEEN THE DIFFUSION MAPS.

Maps	p(AUC)	p(Spe)	p(Se)
FA-MD	<0.001	<0.001	0.042
FA-RD	<0.001	<0.001	0.017
FA-NDI	0.014	0.007	0.004
MD-NDI	<0.001	<0.001	<0.001
RD-NDI	<0.001	<0.001	<0.001
AD-NDI	<0.001	<0.001	<0.001
ODI-NDI	<0.001	<0.001	<0.001

Sensitivity (Sen), specificity (Spec), fractional anisotropy (FA), mean diffusivity (MD), radial diffusivity (RD), axial diffusivity (AD), neurite density index (NDI) and orientation dispersion index (ODI). p-value obtained with Kruskal-Wallis test and a post–hoc with Bonferroni correction.

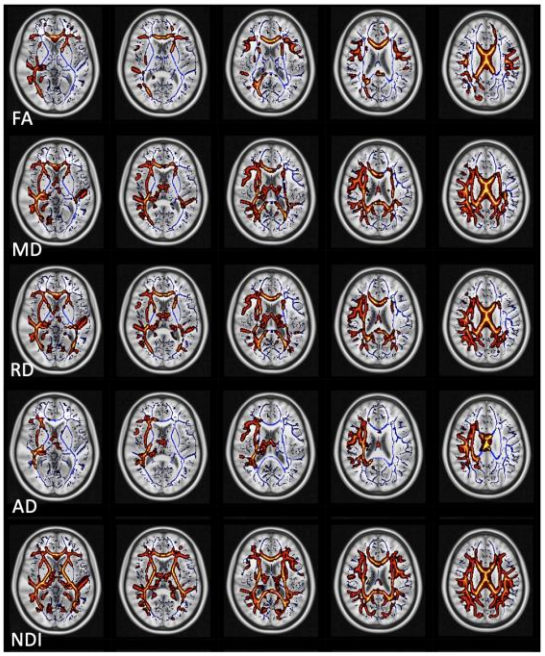

Figure 2. Statistically significant differences in DWI maps between HIV positive patients and healthy control subjects. Blue: FA skeleton extracted from through TBSS analysis. (FA) Red-yellow: lower FA values in HIV positive patients compared to healthy control subjects. (MD) Red-yellow: higher MD values in HIV positive patients compared to healthy control subjects. (RD) Red- yellow: higher RD values in HIV positive patients compared to healthy control subjects. (AD) Red- yellow: higher AD values in HIV positive patients compared to healthy control subjects. (NDI) Red-yellow: lower NDI values in HIV positive patients compared to healthy control subjects.

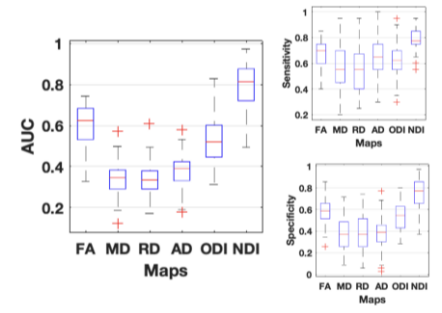

Figure 3. Box-and-whisker plots across ROIs showing AUC, Sensitivity and Specificity for fractional anisotropy (FA), mean diffusivity (MD), radial diffusivity (RD), axial diffusivity (AD), neurite density index (NDI) and orientation dispersion index (ODI) for discriminating between HIV positive patients and healthy controls.

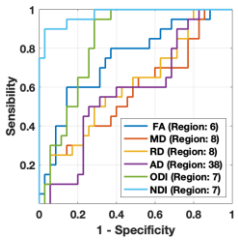

Figure 4. ROC curves relative to the highes AUC we found across ROIs using separately fractional anisotropy (FA), mean diffusivity (MD), radial diffusivity (RD), axial diffusivity (AD), neurite density index (NDI) and orientation dispersion index (ODI) in the differentiation task between HIV patients and healthy controls.

IV. Discussion and Conclusion

When comparing HIV-infected patients to healthy controls, the NODDI model showed more widespread brain involvement as compared to DTI model, also yielding a better overall discrimination performance. The brain structures in which NODDI-related indices were significantly different are related to multimodal associative brain areas whose functions (memory, attentive and emotional networks) are known to be often compromised in HIV positive patients [36], [37], hence offering a mechanistic explanation for these impairments. In addition, the NODDI model highlighted the involvement of the infratentorial structures, possibly related to the neurological impairments which can occur in HIV patients [37]. Finally, the superior discrimination accuracy of NODDI derived indices within a clinically feasible scan time makes it a possible candidate, neuroimaging-related biomarker for HIV studies where monitoring of brain involvement is desired.

References

[1] Y. Assaf, H. Johansen-Berg, and M. Thiebaut de Schotten, "The role of diffusion MRI in neuroscience," *NMR in Biomedicine*. 2019.

[2] A. R. Padhani *et al.*, "Diffusion-weighted magnetic resonance imaging as a cancer biomarker: Consensus and recommendations," in *Neoplasia*, 2009.

[3] M. Mascalchi, M. Filippi, R. Floris, C. Fonda, R. Gasparotti, and N. Villari, "Diffusion-weighted MR of the brain: methodology and clinical application.," *La Radiologia medica*. 2005.

[4] S. Minosse, S. Marzi, F. Piludu, and A. Vidiri, "Correlation study between DKI and conventional DWI in brain and head and neck tumors," *Magn. Reson. Imaging*, 2017.

[5] A. Vidiri *et al.*, "Cervical lymphadenopathy: can the histogram analysis of apparent diffusion coefficient help to differentiate between lymphoma and squamous cell carcinoma in patients with unknown clinical primary tumor?," *Radiol. Medica*, 2019.

[6] A. Vidiri *et al.*, "Feasibility study of reduced field of view diffusion-weighted magnetic resonance imaging in head and neck tumors," *Acta radiol.*, 2017.

[7] D. S. Novikov, E. Fieremans, S. N. Jespersen, and V. G. Kiselev, "Quantifying brain microstructure with diffusion MRI: Theory and parameter estimation," *NMR in Biomedicine*. 2019.

[8] F. Garaci *et al.*, "Brain MR diffusion tensor imaging in Kennedy's disease," *Neuroradiol. J.*, 2015.

[9] Y. Assaf and O. Pasternak, "Diffusion tensor imaging (DTI)-based white matter mapping in brain research: A review," *Journal of Molecular Neuroscience*. 2008.

[10] S. Marzi, S. Minosse, A. Vidiri, F. Piludu, and M. Giannelli, "Diffusional kurtosis imaging in head and neck cancer: On the use of trace-weighted images to estimate indices of non-Gaussian water diffusion," *Med. Phys.*, 2018.

[11] S. Minosse *et al.*, "Diffusion kurtosis imaging in head and neck cancer: A correlation study with dynamic contrast enhanced MRI," *Phys. Medica*, 2020.

[12] A. Conti, M. Palombo, A. Parmentier, G. Poggi, P. Baglioni, and F. De Luca, "Two-phase water model in the cellulose network of paper," *Cellulose*, 2017.

[13] H. Zhang, T. Schneider, C. A. Wheeler-Kingshott, and D. C. Alexander, "NODDI: Practical in vivo neurite orientation dispersion and density imaging of the human brain," *Neuroimage*, 2012.

[14] H. Fukutomi *et al.*, "Diffusion Tensor Model links to Neurite Orientation Dispersion and Density Imaging at high b-value in Cerebral Cortical Gray Matter," *Sci. Rep.*, 2019.

[15] K. Kamiya, M. Hori, and S. Aoki, "NODDI in clinical research," *Journal of Neuroscience Methods*. 2020.

[16] Y. Kadota *et al.*, "Differentiation between glioblastoma and solitary brain metastasis using neurite orientation dispersion and density imaging," *J. Neuroradiol.*, 2020.

[17] M. Rostampour, H. Hashemi, S. M. Najibi, and M. A. Oghabian, "Detection of structural abnormalities of cortical and subcortical gray matter in patients with MRI-negative refractory epilepsy using neurite orientation dispersion and density imaging," *Phys. Medica*, 2018.

[18] T. D. Parker *et al.*, "Cortical microstructure in young onset Alzheimer's disease using neurite orientation dispersion and density imaging," *Hum. Brain Mapp.*, 2018.

[19] A. R. Mayer, J. M. Ling, A. B. Dodd, T. B. Meier, F. M. Hanlon, and S. D. Klimaj, "A prospective microstructure imaging study in mixed-martial artists using geometric measures and diffusion tensor imaging: methods and findings," *Brain Imaging Behav.*, 2017.

[20] F. Grussu *et al.*, "Neurite dispersion: a new marker of multiple sclerosis spinal cord pathology?," *Ann. Clin. Transl. Neurol.*, 2017.

[21] A. Mastropietro *et al.*, "Microstructural characterization of corticospinal tract in subacute and chronic stroke patients with distal lesions by means of advanced diffusion MRI," *Neuroradiology*, 2019.

[22] E. E. O'Connor, A. Jaillard, F. Renard, and T. A. Zeffiro, "Reliability of white matter microstructural changes in HIV infection: Meta-analysis and confirmation," *Am. J. Neuroradiol.*, 2017.

[23] R. li Li, J. Sun, Z. chao Tang, J. ji Zhang, and H. jun Li, "Axonal chronic injury in treatment-naïve HIV+ adults with asymptomatic neurocognitive impairment and its relationship with clinical variables and cognitive status," *BMC Neurol.*, 2018.

[24] O. Davies *et al.*, "Clinical and neuroimaging correlates of cognition in HIV," *J. Neurovirol.*, 2019.

[25] R. P. Bell, L. L. Barnes, S. L. Towe, N. kuei Chen, A. W. Song, and C. S. Meade, "Structural connectome differences in HIV infection: brain network segregation associated with nadir CD4 cell count," *J. Neurovirol.*, 2018.

[26] F. Garaci *et al.*, "Cerebral Multishell Diffusion Imaging Parameters are Associated with Blood Biomarkers of Disease Severity in HIV Infection," *J. Neuroimaging*, 2019.

[27] A. M. Behrman-Lay, R. H. Paul, J. Heaps-Woodruff, L. M. Baker, C. Usher, and B. M. Ances, "Human immunodeficiency virus has similar effects on brain volumetrics and cognition in males and females," *J. Neurovirol.*, 2016.

[28] D. G. Corrêa *et al.*, "Diffusion tensor MR imaging of white matter integrity in HIV-positive patients with planning deficit," *Neuroradiology*, 2015.

[29] J. M. Heaps-Woodruff, P. W. Wright, B. M. Ances, D. Clifford, and R. H. Paul, "The impact of human immune deficiency virus and hepatitis C coinfection on white matter microstructural integrity," *J. Neurovirol.*, 2016.

[30] M. Jenkinson, C. F. Beckmann, T. E. J. Behrens, M. W. Woolrich, and S. M. Smith, "FSL - Review," *Neuroimage*, 2012.

[31] R. L. Harms, F. J. Fritz, A. Tobisch, R. Goebel, and A. Roebroeck, "Robust and fast nonlinear optimization of diffusion MRI microstructure models," *Neuroimage*, 2017.

[32] R. L. Harms and A. Roebroeck, "Robust and fast markov chain monte carlo sampling of diffusion MRI microstructure models," *Front. Neuroinform.*, 2018.

[33] S. Mori *et al.*, "Stereotaxic white matter atlas based on diffusion tensor imaging in an ICBM template," *Neuroimage*, 2008.

[34] S. M. Smith *et al.*, "Tract-based spatial statistics: Voxelwise analysis of multi-subject diffusion data," *Neuroimage*, 2006.

[35] S. M. Smith and T. E. Nichols, "Threshold-free cluster enhancement: Addressing problems of smoothing, threshold dependence and localisation in cluster inference," *Neuroimage*, 2009.

[36] S. Minosse *et al.*, "Disruption of brain network organization in patients with human immunodeficiency virus (HIV) infection," 2020, pp. 1726–1729.

[37] S. Minosse *et al.*, "Functional brain network reorganization in HIV infection," *J. Neuroimaging*, no. December 2020, pp. 1–13, 2021.